


Article

Photosynthetic Processes and Light Response Model Fitting of *Quercus acutissima* Carruth. and *Quercus variabilis* Bl. in the Changjiang River Delta, China

Cunxin Ruan ^{1,2} , Haibo Hu ^{1,2,*}, Can Cheng ^{1,2}, Pei Fang ², Xichuan Jia ², Zhaoming Wu ³ and Li Zhu ³

¹ Co-Innovation Center for the Sustainable Forestry in Southern China, Nanjing Forestry University, Nanjing 210037, China

² Key Laboratory of Soil and Water Conservation and Ecological Restoration in Jiangsu Province, Nanjing Forestry University, Nanjing 210037, China

³ Wuxi Branch, Bureau of Investigation on Hydrologic Water Resources, Wuxi 214100, China

* Correspondence: huhb2000@aliyun.com

Abstract: Plants have the capacity to fix CO₂ through photosynthesis. To reveal the photosynthetic processes of *Quercus acutissima* Carruth. and *Quercus variabilis* Bl., their net photosynthetic rates were quantified during the early and peak growing seasons. To evaluate forest photosynthetic efficiencies, the photosynthetic light response curves of *Q. acutissima* and *Q. variabilis* were fitted by the rectangular hyperbola model (RHM), non-rectangular hyperbola model (NHM), and modified rectangular hyperbola model (Ye model). The results revealed the following: (1) All daily variation curves of the net photosynthetic rate, stomatal conductivity, and transpiration rate were single-peaked. The peak times of the *Q. acutissima* and *Q. variabilis*' net photosynthetic rates appeared at 12:00 a.m. during the early growing season and 10:00 a.m. during the peak growing season. (2) The photosynthetic capacities of both *Q. acutissima* and *Q. variabilis* during peak growing seasons were higher than during the early growing season. (3) The net photosynthetic rate was found to be positively correlated with stomatal conductivity, the transpiration rate, and photosynthetically active radiation, and it was negatively correlated with the intercellular CO₂ concentration. (4) The Ye model provided the best fit for the light response curves of *Q. acutissima* and *Q. variabilis* when compared with the rectangular hyperbola and nonrectangular hyperbola models. The photosynthetic performance of *Q. acutissima* was superior to that of *Q. variabilis*; thus, it can be employed as a priority tree species in carbon sink forests.

Keywords: photosynthetic rate; photosynthetic efficiency; photosynthetic light response model; *Q. acutissima*; *Q. variabilis*



Citation: Ruan, C.; Hu, H.; Cheng, C.; Fang, P.; Jia, X.; Wu, Z.; Zhu, L. Photosynthetic Processes and Light Response Model Fitting of *Quercus acutissima* Carruth. and *Quercus variabilis* Bl. in the Changjiang River Delta, China. *Forests* **2022**, *13*, 2010. <https://doi.org/10.3390/f13122010>

Academic Editor: Ilona Mészáros

Received: 12 October 2022

Accepted: 24 November 2022

Published: 28 November 2022

Publisher's Note: MDPI stays neutral with regard to jurisdictional claims in published maps and institutional affiliations.



Copyright: © 2022 by the authors. Licensee MDPI, Basel, Switzerland. This article is an open access article distributed under the terms and conditions of the Creative Commons Attribution (CC BY) license (<https://creativecommons.org/licenses/by/4.0/>).

1. Introduction

Photosynthesis is a biological process that absorbs CO₂ and releases O₂ to balance their concentrations in the ambient atmosphere [1]. Through photosynthesis, forests serve as an important carbon sink for terrestrial ecosystems by fixing CO₂ [2]. Photosynthetic parameters are essential indicators for the evaluation of forest photosynthetic efficiencies. The photosynthetic light response method is an important research technique in plant physiology [3]. From light response curves, photosynthetic parameters such as the maximum net photosynthetic rate, light saturation point, light compensation point, dark respiration rate, and apparent quantum efficiency can be obtained. The photosynthesis of plants is also affected by their physiology (e.g., stomatal conductivity) and environmental factors (e.g., photosynthetically active radiation) [4–6]. As plants grow, the environment, as well as their own physiological conditions, are altered. Subsequently, their photosynthetic capacities change during different growing seasons. Thus, it is critical to elucidate the photosynthetic processes of plants and their impact factors during different growing seasons.

The main models for fitting photosynthetic light response curves include the rectangular hyperbola model (RHM), the nonrectangular hyperbola model (NHM), the Ye-modified model (modified rectangular hyperbola model, YZP), the exponential model, etc. The rectangular hyperbola model was proposed by Baly in 1935, who described the relationship between photosynthesis and irradiance thusly: the net photosynthetic rate increases sharply with greater photosynthetically active radiation under low light intensities and slowly with greater photosynthetically active radiation at moderate light intensities [7]. The rectangular hyperbola model has been applied to simulate the light response curve of *Ziziphus jujuba* Var., *Populus Euramericana* Cv., and *Pinus pinea* L. and achieved good results [8–10]. The nonrectangular hyperbola model was proposed by Thornley in 1976 based on the rectangular hyperbola model with the addition of curvilinear angle (θ) to adjust the curvature of the curve [11]. Lang found that the nonrectangular hyperbola was the best model for fitting the light response curve of *Prunus sibirica* L., *Hippophae rhamnoides* L., and *Pinus tabulaeformis* Carr. [12]. The modified rectangular hyperbola model was proposed by Ye in 2007, which was based on the rectangular hyperbola model with the addition of a limiting parameter (β) to handle photosynthetic inhibition data. Li discovered that the modified rectangular hyperbola model could well fit the photosynthetic light response curve under a wide range of soil water conditions [13]. The rectangular hyperbola and nonrectangular hyperbola models are good at fitting the light compensation point and apparent quantum efficiency. The photosynthetic parameters fitted by the Ye model describe not only the light response characteristics but also the molecular photosynthetic pigment characteristics [14] and reproduce the light response trends of electron transport and CO₂ absorption [15]. Previous studies on photosynthetic light response curves showed that there were differences in fitting the photosynthetic parameters of the same plant using different models. Thus, it is of particular importance to select the optimal light response model to investigate the photosynthetic attributes of plants [16]. For this study, based on earlier research and our preliminary validations [17,18], we selected rectangular hyperbola, nonrectangular hyperbola, and Ye-modified models to fit the light response curves.

Quercus acutissima Carruth. and *Quercus variabilis* Bl. are widespread across warm temperate and subtropical regions of China. They are important, highly adaptable tree species with strong water conservation and excellent carbon sequestration capacities. These trees are extensively distributed throughout the Yangtze River Delta region and are broadly accepted by researchers as carbon sink trees [19,20]. The Yangtze River Delta region is an important area affected by acid rain, with a 57.12% acid precipitation frequency [21]. Most previous studies into the photosynthetic parameters of *Quercus acutissima* and *Quercus variabilis* involved saplings [22,23], some of which were concentrated in arid and high-temperature regions [24]. Further, they were situated in regions that were less affected by acid rain, while leaf photosynthesis was impacted by acid rain to a certain extent [25]. It is very important to understand the photosynthetic capacities of *Quercus acutissima* and *Quercus variabilis* in this region.

For this study, we continuously observed the photosynthetic diurnal variations of *Q. acutissima* and *Q. variabilis* in the Changjiang River Delta region for different growing seasons and simulated their photosynthetic light response curves using the rectangular hyperbola, nonrectangular hyperbola, and Ye models. This study endeavored to explore the photosynthetic processes and relationships between photosynthesis and eco-physiological factors. Secondly, we aimed to select an optimal model to simulate the light response curves of *Q. acutissima* and *Q. variabilis*. Finally, we selected highly photosynthetically efficient *Quercus* spp. plants. Our results revealed the photosynthetic capacities of oak forests in the Yangtze Delta region and evaluated the photosynthetic efficiencies of individual oak trees. Further, this study provided a scientific basis to support the further study of forest carbon fixation in acid rain-impacted areas.

2. Materials and Methods

2.1. Site Description

This study was conducted at the Changjiang River Delta Forest Ecosystem National Positioning Station (E119°12′03″, N32°07′48″, 332.6 m) of the State Forestry and Grassland Administration. The site inhabits the middle foothills of Hollow Green Mountain, with a 20° southeast slope, in Jurong City, Jiangsu Province, East China (Figure 1), under a north subtropical monsoon climate. The mean annual temperature in this area is 15.2 °C, the mean frost-free period is 233 d, and the mean annual precipitation is 1055.6 mm. The soil is yellow-brown loam at pH 4.76 [26]. The dominant tree species are sawtooth oak (*Q. acutissima*) and oriental oak (*Q. variabilis*), with a small population of maple (*Liquidambar formosara*), Chinese pistache (*Pistacia chinensis*), etc. The basic characteristics of the forest stands are shown in Table 1.

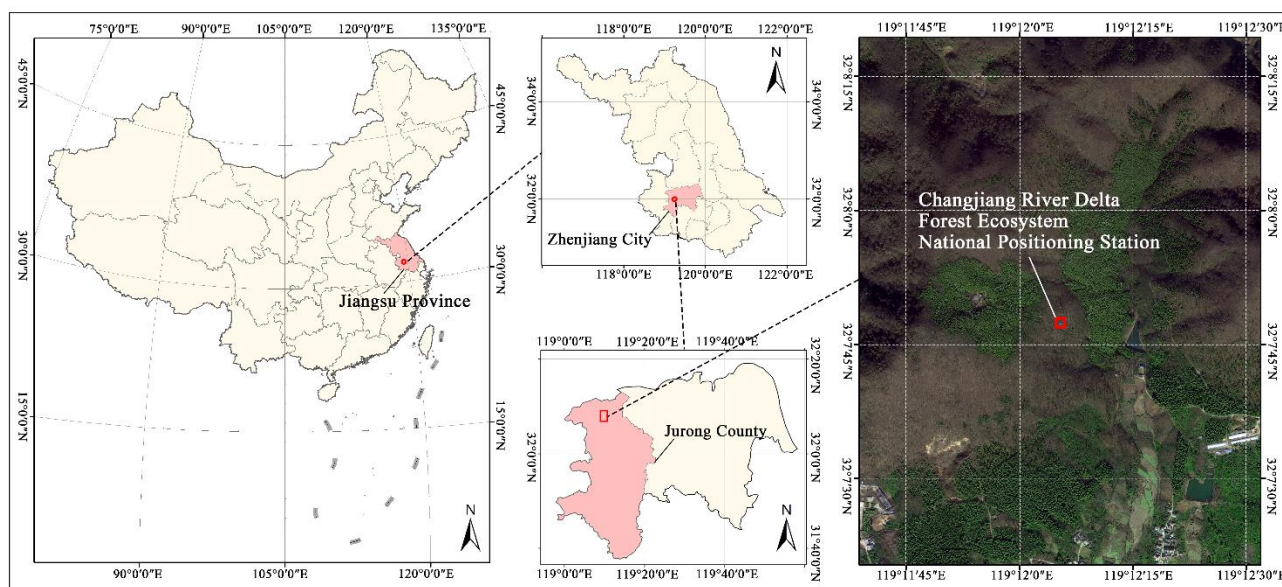


Figure 1. Study site location map. The study site is in Jurong County, Zhenjiang City, Jiangsu Province, China. Red rectangle identifies the sampling site. Because the remote sensing satellite map was obtained in the winter, it appears brown in the red rectangle.

Table 1. Basic characteristics of sample stands. Three sample squares of 20 m × 20 m were set up, wherein every 27 trees was measured.

Tree Species	<i>Q. acutissima</i>	<i>Q. variabilis</i>
Forest age/years	65	65
Tree height/m	19.24	17.78
Diameter/cm	26.64	25.08
Crown/m	4.6	4.1
Density/plants·hm ⁻²	325	350
Crown density	0.5	0.47

Note: The forest survey was implemented according to the National Standard of the People's Republic of China's "Long-term positioning observation method of forest ecosystem" (GB/T33027-2016).

2.2. Climate Observation

The climate was observed continuously for 24 h every day for the entire year. The main meteorological factors observed at the experimental site were photosynthetically active radiation (PAR) ($\mu\text{mol m}^{-2} \text{s}^{-1}$) and air temperature (°C). The photosynthetically active radiation was measured using a radiation sensor SK01-DP2 (MIDDLETON SOLAR Inc., Melbourne, VIC, Australia), while the air temperature was quantified with a thermo-

hygrometer HMP155A (VAISALA Inc., Helsinki, Finland), which were both at 20 m above the ground surface (observation tower).

2.3. Measurement of Photosynthetic Characteristics and Light Response Curve

From 20 to 28 April and 6 to 14 July (both with clear skies), photosynthetic characteristic measurements were obtained every two hours from 6:00 a.m. to 18:00 p.m. using a portable photosynthesizer LI-6400 (LI-COR Inc., Lincoln, OR, USA). Three healthy and fully expanded leaves were selected from the middle of the canopies of six standard *Q. acutissima* and *Q. variabilis* trees with height and diameter at breast height close to average values. The net photosynthetic rate, intercellular CO₂ concentration, transpiration rates, and stomatal conductivities were measured simultaneously. Finally, the arithmetic averages of the measurements were used as photosynthetic data for the early peak growing season (20 April to 30 May) and the peak growing season (1 July to 30 August), respectively. During the early growing season, the temperature ranged from 15 to 25 °C, air humidity from 34% to 50%, CO₂ concentration from 375 to 398 µmol mol⁻¹, and PAR from 1 to 1300 µmol m⁻² s⁻¹. During the peak growing season, the temperature ranged from 20 to 35 °C, air humidity from 45% to 91%, CO₂ concentration from 370 to 398 µmol mol⁻¹, and PAR from 1 to 1600 µmol m⁻² s⁻¹.

According to numerous studies, the most sensitive time for plant photosynthesis in response to light intensity is between 9:00 a.m. and 11:00 a.m. [27–29]. Consequently, for this study, we selected three leaves from three healthy *Q. acutissima* and *Q. variabilis* trees and made measurements from 9:00 a.m. to 11:00 a.m. each day under clear skies from 6 to 14 July. The sample chamber conditions were controlled, with the leaf temperature set at 25 °C, relative air humidity set at 60%, atmospheric CO₂ concentration set at 400 µmol mol⁻¹, an airflow rate of about 500 µmol s⁻¹, and light radiation intensities set at 0, 10, 20, 50, 100, 200, 400, 600, 800, 1000, 1200, 1400, 1600, 1800, and 2000 µmol m⁻² s⁻¹. Once the light intensities were adjusted, the leaves remained in the sample chamber for two min, with measurement times no less than two minutes.

2.4. Fitting Model of the Photosynthetic Light Response Curve

The photosynthetic light response curves of *Q. acutissima* and *Q. variabilis* were fitted using the rectangular hyperbola, nonrectangular hyperbola, and Ye models. The net photosynthetic rates and photosynthetically active radiation curves were quantified [30], while the maximum net photosynthetic rate, light compensation point, light saturation point, and dark respiration rate were estimated from the curve trend as the measured values of the characteristic parameters of light responses [12,31].

The rectangular hyperbola model (RHM) equation was expressed as follows:

$$P_n = \frac{\alpha I P_{n\max}}{\alpha I + P_{n\max}} - R_d \quad (1)$$

where P_n is the net photosynthetic rate (µmol m⁻² s⁻¹), α is the initial quantum efficiency, I is the photosynthetic active radiation intensity (µmol m⁻² s⁻¹), $P_{n\max}$ is the maximum net photosynthetic rate at light saturation (µmol m⁻² s⁻¹), and R_d is the dark respiration rate (µmol m⁻² s⁻¹)

The nonrectangular hyperbolic model (NHM) equation was expressed as follows:

$$P_n = \frac{\alpha I + P_{n\max} - \sqrt{(\alpha I + P_{n\max})^2 - 4\alpha\theta I P_{n\max}}}{2\theta} - R_d \quad (2)$$

where θ is the optical response curve angle of the curvature, with the other letters referring to the same as above.

The Ye model (the modified rectangular hyperbola model, YZP) equation was expressed as follows:

$$P_n = \alpha \frac{1 - \beta I}{1 + \gamma I} I - R_d \quad (3)$$

where β is the photoinhibition coefficient ($\text{m}^2 \text{s} \mu\text{mol}^{-1}$), γ is the light saturation coefficient ($\text{m}^2 \text{s} \mu\text{mol}^{-1}$), and the other letters have the same meanings as above.

The light saturation points, I_s ($\mu\text{mol m}^{-2} \text{s}^{-1}$), for the rectangular hyperbola and nonrectangular hyperbola models were calculated using the equation below [32]. First, a linear regression of the photosynthetic active radiation, I , from 0 to 200 ($\mu\text{mol m}^{-2} \text{s}^{-1}$) and the net photosynthetic rate, P_n , were used to obtain the apparent quantum efficiency (AQE) and dark respiration rate (R_d), with the equation expressed as follows:

$$P_n = m \times I - R_d \quad (4)$$

where P_n is the net photosynthetic rate ($\mu\text{mol m}^{-2} \text{s}^{-1}$), slope m is apparent quantum efficiency, and the R_d is the dark respiration rate ($\mu\text{mol m}^{-2} \text{s}^{-1}$).

Then, the light saturation point, I_s , was calculated with Equation (4):

$$I_s = \frac{P_{n\max} + R_d}{m} \quad (5)$$

where $P_{n\max}$ is the max net photosynthetic rate ($\mu\text{mol m}^{-2} \text{s}^{-1}$), m is apparent quantum efficiency, and R_d is dark respiration rate ($\mu\text{mol m}^{-2} \text{s}^{-1}$).

The light saturation point, I_s , in the Ye model was expressed as follows:

$$I_s = \frac{\sqrt{(\beta + \gamma)/\beta} - 1}{\gamma} \quad (6)$$

where the net photosynthetic rate P_n is 0, and the light compensation point (I_c) ($\text{mol m}^{-2} \text{s}^{-1}$) is the photosynthetically active radiation. As a result, for the RHM, NHM, and YZP models, the P_n was set to 0 to obtain the respective I_c values.

The formula of the light compensation point for the rectangular hyperbola model was expressed as follows:

$$I_c = \frac{R_d P_{n\max}}{\alpha(P_{n\max} - R_d)} \quad (7)$$

The formula of the light compensation point for the nonrectangular hyperbolic model was expressed as follows:

$$I_c = \frac{P_{n\max} R_d - \theta R_d^2}{\alpha(P_{n\max} - R_d)} \quad (8)$$

The formula of the light compensation point, for the Ye model was expressed as follows:

$$I_c = \frac{\alpha - R_d \gamma - \sqrt{(\alpha - R_d \gamma)^2 - 4\alpha\beta R_d}}{2\alpha\beta} \quad (9)$$

The maximum net photosynthetic rate equation for the Ye model was expressed as follows:

$$P_{n\max} = \alpha \left(\frac{\sqrt{\beta + \gamma} - \sqrt{\beta}}{\gamma} \right)^2 - R_d \quad (10)$$

2.5. Model Evaluation

To evaluate the goodness of fit for the three models, the root-mean-square error (RMSE), mean absolute percentage error (MAPE), and determination coefficient (R^2) were calculated using empirical formulae. The determination coefficient was established by fitting the light response curve with Matlab 2020, while the RMSE and MAPE were calculated using the equations below [33]:

$$RMSE = \sqrt{\frac{1}{n} \sum_{i=1}^n (Y_{m,i} - Y_{0,i})^2} \quad (11)$$

where $Y_{m,i}$ is the predicted value of the model, and $Y_{0,i}$ is the observed value, as shown below:

$$MAPE = \frac{1}{n} \sum_{i=1}^n \left| \frac{Y_{m,i} - Y_{0,i}}{Y_{0,i}} \right| \times 100\% \quad (12)$$

2.6. Data Analysis

The net photosynthetic rate and eco-physiological factor data were processed using Excel 2017 and SPSS (V 19, Armonk, NY, USA) for correlation analysis. Origin software (Version 2018, Northampton, MA, USA) was employed to plot the dynamic photosynthetic daily change characteristics and photosynthetic light response curves. Matlab software (Version 2020, Natick, MA, USA) was employed to build the rectangular hyperbola, nonrectangular hyperbola, and Ye models.

3. Results

3.1. Diurnal Dynamics of Photosynthetic Parameters

3.1.1. Diurnal Variations of Net Photosynthetic Rates

The daily trend of the net photosynthetic rates of *Q. acutissima* and *Q. variabilis* was a single-peaked curve for both the early and peak growing seasons, as shown in Figure 2A. During the early growing season, the peak net photosynthetic rates of *Q. acutissima* and *Q. variabilis* were 4.40 and 4.07 $\mu\text{mol m}^{-2} \text{s}^{-1}$, respectively, and the peak time appeared at 12:00 a.m. During the peak growing season, the peak net photosynthetic rates of *Q. acutissima* and *Q. variabilis* were 6.87 and 5.05 $\mu\text{mol m}^{-2} \text{s}^{-1}$, respectively, and the peak time appeared at 10:00 a.m. The peak net photosynthetic rate during the peak growing season occurred two hours earlier than during the early growing season, and the mean daily net photosynthetic rates of both *Q. acutissima* and *Q. variabilis* during the peak growing season were higher than during the early growing season. The average daily net photosynthetic rate of 1.94 $\mu\text{mol m}^{-2} \text{s}^{-1}$ was higher than that of *Q. variabilis* (1.86 $\mu\text{mol m}^{-2} \text{s}^{-1}$) during the early growing season but not significant ($p = 0.12$). During the peak growing season, the average daily net photosynthetic rate of *Q. acutissima* was 4.16 $\mu\text{mol m}^{-2} \text{s}^{-1}$, compared with 3.10 $\mu\text{mol m}^{-2} \text{s}^{-1}$ for *Q. variabilis*.

3.1.2. Diurnal Variation of Transpiration Rate

Plant transpiration is intimately linked to photosynthesis, which facilitates carbon assimilation and the diffusion and transportation of CO_2 from the ambient atmosphere to leaf flesh cells. As illustrated in Figure 2D, the daily trends of *Q. acutissima* and *Q. variabilis* transpiration were consistent with the photosynthetic rate (both in a single-peaked pattern), whereas the peak transpiration rate for *Q. acutissima* occurred at 12:00 at 0.80 $\text{mol m}^{-2} \text{s}^{-1}$ during the early growing season, with a daily mean transpiration rate of 0.377 $\text{mol m}^{-2} \text{s}^{-1}$. The peak transpiration rate of *Q. variabilis* also occurred at 12:00 a.m. at 0.67 $\text{mol m}^{-2} \text{s}^{-1}$, whereas the daily mean transpiration rate was 0.36 $\text{mol m}^{-2} \text{s}^{-1}$. The peak transpiration rate for *Q. acutissima* appeared at 12:00 at 0.06 $\text{mol m}^{-2} \text{s}^{-1}$, and the daily mean transpiration rate was 1.11 $\text{mol m}^{-2} \text{s}^{-1}$ during the peak growing season. The peak transpiration rate for *Q. variabilis* occurred at 12:00 a.m. at 0.05 $\text{mol m}^{-2} \text{s}^{-1}$, and the mean daily transpiration rate was 0.91 $\text{mol m}^{-2} \text{s}^{-1}$. The daily mean transpiration rates of *Q. acutissima* and *Q. variabilis* during the peak growing season were higher than those of the early growing season, with the transpiration rate of *Q. acutissima* being higher than that of *Q. variabilis*.

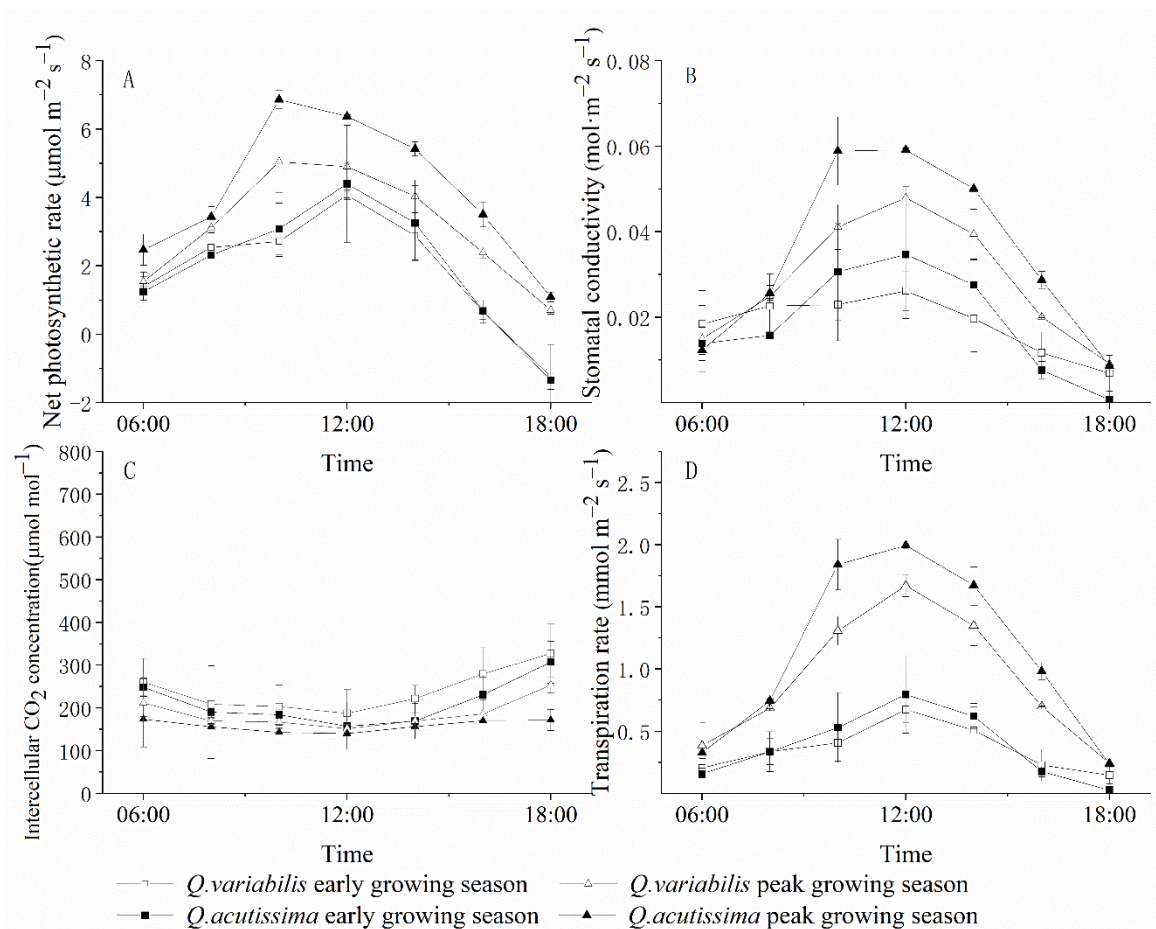


Figure 2. Diurnal variation of photosynthetic characteristics of *Quercus acutissima* Carruth. and *Quercus variabilis* Bl. during early and peak growing seasons. (A) Diurnal variation of net photosynthetic rate ($\mu\text{mol m}^{-2} \text{s}^{-1}$). (B) Diurnal variation of stomatal conductivity ($\text{mol m}^{-2} \text{s}^{-1}$). (C) Diurnal variation of intercellular CO_2 concentration $\mu\text{mol mol}^{-1}$. (D) Diurnal variation of transpiration rate ($\text{mmol m}^{-2} \text{s}^{-1}$).

3.1.3. Diurnal Variation of Stomatal Conductivity

Stomata are the channels through which CO_2 and water ingress and egress leaves, where stomatal conductivity reflects the capacity of leaves to exchange CO_2 and water with the ambient environment. The daily variation of stomatal conductivity was unimodal (Figure 2B) and corresponded to the daily trend of the net photosynthetic and transpiration rates. The daily average stomatal conductivities of *Q. acutissima* and *Q. variabilis* were lower during the early growing season than during the peak growing season. At 12:00 a.m., the peak stomatal conductivity of *Q. acutissima* was $0.03 \text{ mol m}^{-2} \text{ s}^{-1}$, whereas that of *Q. variabilis* was $0.03 \text{ mol m}^{-2} \text{ s}^{-1}$. The peak stomatal conductivity of *Q. acutissima* was $0.06 \text{ mol m}^{-2} \text{ s}^{-1}$ at 12:00 a.m. and $0.05 \text{ mol m}^{-2} \text{ s}^{-1}$ at 12:00 a.m. during the peak growing season. The mean daily stomatal conductivity for *Q. acutissima* was $0.02 \text{ mol m}^{-2} \text{ s}^{-1}$ and $0.02 \text{ mol m}^{-2} \text{ s}^{-1}$ for *Q. variabilis* during the early growing season. During the peak growing season, the mean daily stomatal conductivity was $0.03 \text{ mol m}^{-2} \text{ s}^{-1}$ for *Q. acutissima* and $0.03 \text{ mol m}^{-2} \text{ s}^{-1}$ for *Q. variabilis*.

3.1.4. Diurnal Variation of Intercellular CO_2

Intercellular CO_2 is the primary raw material for photosynthesis in leaves, where its concentration reflects its strength. As shown in Figure 2C, the daily intercellular variations in CO_2 exhibited a trend of being low in the afternoon and high in the morning and evening during both the early growth and peak seasons. Figure 2 reveals that, as the solar radiation

increased, leaf photosynthesis commenced, after which the intercellular CO₂ concentration gradually decreased to reach its low point at midday. The lowest CO₂ concentrations for *Q. acutissima* and *Q. variabilis* were 157.18 and 187.25 $\mu\text{mol mol}^{-1}$, respectively, during the early growing season and 140.25 and 151.70 $\mu\text{mol mol}^{-1}$, respectively, during the peak growing season. The concentration of intercellular CO₂ steadily increased as photosynthesis weakened in the afternoon. During the early growing season, the average intercellular CO₂ concentrations for *Q. acutissima* and *Q. variabilis* were 212.36 and 241.27 $\mu\text{mol mol}^{-1}$, respectively. During the peak growing season, the intercellular CO₂ concentrations for *Q. acutissima* and *Q. variabilis* were 158.61 and 187.01 $\mu\text{mol mol}^{-1}$, respectively. The concentration of intercellular CO₂ for *Q. variabilis* was higher than that of *Q. acutissima* during both the early and peak growing seasons. Furthermore, with more robust photosynthesis, the intercellular CO₂ concentration was lower. As shown in Figure 2C, the intercellular CO₂ concentrations of *Q. acutissima* and *Q. variabilis* reached a valley at 10:00 a.m., in conjunction with the peaking net photosynthetic rate.

3.1.5. Correlation Analysis of Net Photosynthetic Rate and Eco-Physiological Factors

We observed physiological indicators such as the net photosynthetic rate, stomatal conductivity, and transpiration rate, as well as associated environmental factors, including photosynthetically active radiation (PAR) and temperature, during the early and peak growing seasons. To better comprehend how the net photosynthetic rate responded to eco-physiological factors, it was correlated with the stomatal conductivity, intercellular CO₂ concentration, transpiration rate, photosynthetically active radiation, and air temperature (Table 2). The net photosynthetic rate was found to be significantly positively correlated with the stomatal conductivity, transpiration rate, and photosynthetically active radiation ($p < 0.01$); significantly negatively correlated with the intercellular CO₂ concentration ($p < 0.01$); and insignificantly correlated with the temperature ($p < 0.05$). The strongest correlation was found between the net photosynthetic rate and stomatal conductivity, and the correlation coefficient increased over time. The correlation coefficient between the net photosynthetic rate and stomatal conductivity was 0.89 during the early growing season and 0.98 during the peak growing season, which indicated that the stomatal conductivity had an increased effect on the net photosynthetic rate during the peak growing season. During both the early and peak growing seasons, the correlation coefficient between the net photosynthetic rate and transpiration rate of *Q. acutissima* was greater than that of *Q. variabilis*, which was consistent with the response pattern of the net photosynthetic rate on the stomatal conductivity of *Q. acutissima*. The correlation coefficients between the net photosynthetic rate and stomatal conductivity for *Q. acutissima* and *Q. variabilis* were greater than those between the net photosynthetic rate and photosynthetically active radiation. This implied that the stomatal conductivity had a greater impact on the net photosynthetic rate than the photosynthetically active radiation.

Table 2. Correlation coefficients between net photosynthetic rate and eco-physiological factors during different growing seasons. PAR: photosynthetically active radiation. Significant values are indicated: **, $p < 0.01$.

Species	Growing Period	Stomatal Conductivity	Internal CO ₂ Concentration	Transpiration Rate	Air Temperature	PAR
<i>Q. acutissima</i>	Early	0.890 **	−0.789 **	0.854 **	0.202	0.789 **
	Peak	0.980 **	−0.650 **	0.968 **	0.258	0.626 **
<i>Q. variabilis</i>	Early	0.748 **	−0.737 **	0.617 **	0.281	0.510 **
	Peak	0.942 **	−0.776 **	0.944 **	0.295	0.598 **

3.1.6. Photosynthetic Light Response Model and Photosynthetic Parameters

The dynamic variations in the photosynthetic light response curve for the three models were similar when the PAR was $< 200 \mu\text{mol m}^{-2} \text{s}^{-1}$ (Figure 3B–D). Specifically, the net

photosynthetic rate increased rapidly with greater photosynthetically active radiation, and the predicted values fitted by the three models were close to those measured. When the PAR was $>200 \mu\text{mol m}^{-2} \text{s}^{-1}$, the imitative effects of the three photosynthetic light response models on the light response curves were varied. In the Ye model, the net photosynthetic rates of *Q. acutissima* and *Q. variabilis* gradually decreased when the PAR exceeded the light saturation point (Figure 3D). In the rectangular hyperbola model, the net photosynthetic rate increased slightly as the PAR increased (Figure 3B), whereas in the nonrectangular hyperbola model, the light response curve trended to smoothing. Changes in the photosynthetic light response curve predicted by the Ye model were consistent with the measured curves when the PAR was $>200 \mu\text{mol m}^{-2} \text{s}^{-1}$ (Figure 3A,D).

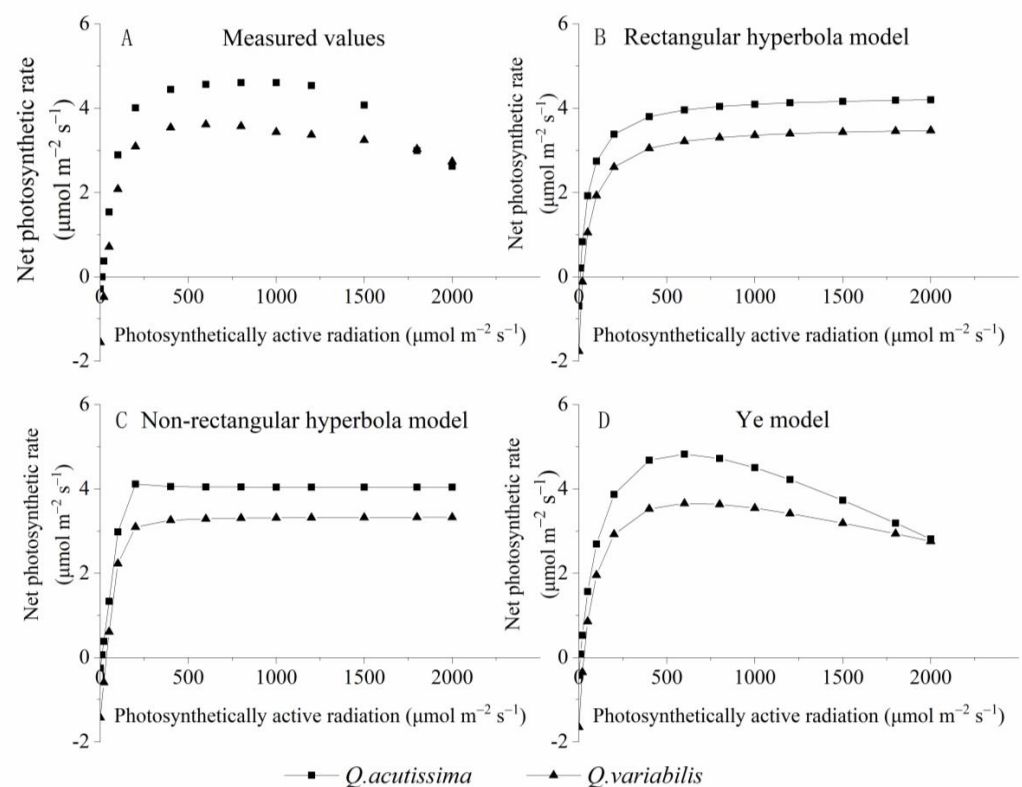


Figure 3. Photosynthetic light response curves of *Q. acutissima* and *Q. variabilis*. (A) Scatter of measured values (B) Simulative curve of Rectangular hyperbola model (C) Simulative Curve of non-rectangular hyperbola model (D) Simulative curve of Ye model.

The light saturation point refers to the light intensity when the photosynthetic intensity of a plant reaches its peak. According to Table 3, the light saturation points (LSP) of the measured curves for *Q. acutissima* and *Q. variabilis* were 783.33 and $666.67 \mu\text{mol m}^{-2} \text{s}^{-1}$, respectively. The ANOVA revealed that the light saturation point of *Q. acutissima* was significantly greater than that of *Q. variabilis* ($p < 0.05$), which meant that *Q. acutissima* utilized more light energy than *Q. variabilis*. The light saturation points of the rectangular hyperbola and nonrectangular hyperbola models for *Q. acutissima* were 62.965% and 78.78% , respectively, which were lower than the measured values, while that of the Ye model was 24.10% lower than the measured values. The light saturation points of the rectangular hyperbola and nonrectangular hyperbola models for *Q. variabilis* were 45.53% and 60.057% lower than the measured values, respectively, while that of the Ye model was 8.62% lower than those measured. This indicated that the light saturation points of the Ye model were closer to the measured values and had a better fit.

Table 3. Photosynthetic parameters of *Quercus acutissima* Carruth. and *Quercus variabilis* Bl. fitted by the three models. Different lowercase letters (i.e., a, b, c) in the same column indicate a significant difference between different models of the same species ($p < 0.05$). Different capital letters (i.e., A, B, C) in the same column indicate a significant difference between different species of the same model ($p < 0.05$). RHM: rectangular hyperbola model; NHM: nonrectangular hyperbola model; YZP: Ye model; LSP: light saturation point; LCP: light compensation point; R_d : dark respiration; and the same below.

Species	Models	LSP/ $\mu\text{mol m}^{-2} \text{s}^{-1}$	LCP/ $\mu\text{mol m}^{-2} \text{s}^{-1}$	$R_d/\mu\text{mol m}^{-2} \text{s}^{-1}$	$P_{nmax}/\mu\text{mol m}^{-2} \text{s}^{-1}$	MAPE/%	RMSE	R^2
<i>Q. acutissima</i>	RHM	296.28bA	7.24aA	0.68cA	5.00aA	20.47	0.68	0.85
	NHM	169.77aA	7.67aA	0.24aA	4.29aA	17.86	0.56	0.90
	YZP	607.24cA	8.14abA	0.42bA	4.85aA	15.37	0.20	0.99
	Measured value	783.33dA	9.86bA	0.29aA	4.65aA	—		
<i>Q. variabilis</i>	RHM	326.84aA	22.67aB	1.76aB	5.36bA	27.18	0.37	0.95
	NHM	239.65aA	34.55aB	1.43aB	4.78abA	25.38	0.24	0.98
	YZP	651.69bA	27.53aB	1.65aB	3.67aB	24.37	0.10	0.99
	Measured value	666.67bB	26.00aB	1.55aB	3.630aB	—		

The minimum light intensity required by plants for photosynthesis is defined as the light compensation point. As shown in Table 3, the light compensation point (LCP) predicted by the rectangular hyperbola model for *Q. acutissima* was $7.24 \mu\text{mol m}^{-2} \text{s}^{-1}$; for the nonrectangular hyperbola model, it was $7.68 \mu\text{mol m}^{-2} \text{s}^{-1}$. These values were 26.55% and 22.18% lower than the measured LCP ($9.86 \mu\text{mol m}^{-2} \text{s}^{-1}$), respectively. The light compensation point predicted by the Ye model ($8.14 \mu\text{mol m}^{-2} \text{s}^{-1}$) was 17.51% lower than the measured value. The LCP predicted by the rectangular hyperbola model for *Q. variabilis* was 12.82% lower than the measured value. Further, the LCP predicted by the nonrectangular hyperbola and Ye models were 32.89% and 5.88% higher, respectively, than the measured value.

For this study, the respiration rate value at a light intensity of zero was used as the measured dark respiration rate. Because of ignoring the photorespiration, the actual dark respiration rate was greater than or equal to the measured respiration rate. The predicted dark respiration rates of the three models for *Q. variabilis* were not significantly different from the measured values. However, for *Q. acutissima*, only the predicted dark respiration rate of the nonrectangular hyperbola model was closer to the measured values, while the predicted dark respiration rates of the rectangular hyperbola and Ye models were 137.02% and 43.94% higher, respectively, than the measured values. According to Table 3, the dark respiration rate of *Q. acutissima* was significantly lower than that predicted or measured for *Q. variabilis* ($p < 0.05$), which was 81.39% lower than for *Q. variabilis*. In the Ye model, *Q. acutissima* had a 74.86% lower dark respiration rate than *Q. variabilis*, where the lower the dark respiration rate, the less CO_2 content was released. This meant that, under the same conditions, *Q. acutissima* had a higher carbon storage capacity than *Q. variabilis*.

The highest net photosynthetic rate was the critical parameter in defining the photosynthetic potential. For the rectangular hyperbola and Ye models of *Q. acutissima*, the maximum net photosynthetic rates predicted were 7.68% and 4.30% greater, respectively, than the measured values. However, there were difference between photosynthetic parameters predicted by different models. The predicted maximum net photosynthetic rate of the rectangular hyperbola model was 47.63% significantly higher than that measured for *Q. variabilis* ($p < 0.05$). While, the predicted maximum net photosynthetic rates of the nonrectangular hyperbola and Ye models were 31.57% ($p = 0.08$) and 1.02% ($p = 0.95$) higher than the measured values, respectively. The measured maximum net photosynthetic rate of *Q. acutissima* was 28.02% higher than that of *Q. variabilis* ($p < 0.05$). Similarly, the maximum net photosynthetic rate of *Q. acutissima* predicted by the Ye model was considerably higher than that of *Q. variabilis* ($p < 0.05$).

The imitative effects of the three models were tested via three indicators, including the root-mean-square error (*RMSE*), mean absolute percentage error (*MAPE*), and coefficient of determination (R^2). The *RMSE* measures the differences between the observed and predicted values and reflects the dispersion of errors. The *MAPE* characterizes the average errors of multiple predictions for evaluating the fitting accuracy of the model to the existing data, while R^2 can determine the degree of model fitting. The lower the *MAPE* and *RMSE*, the closer the R^2 is to one, which indicates a better fit. The *RMSE* of the fitted curves of the three *Q. variabilis* models were 0.37, 0.25, and 0.10, respectively, while the *RMSE* of the fitted curves of the three models for *Q. acutissima* were 0.678, 0.57, and 0.20 respectively. The *RMSE* of the Ye model was the smallest of the three models. In terms of the model-fitting accuracy for the *Q. acutissima* and *Q. variabilis* light response curves, the Ye model had the best fitting accuracy for *Q. acutissima* with an error rate of 15.37%, followed by the nonlinear hyperbolic model with an error rate of 17.86%. The Ye model had the best fitting accuracy for *Q. variabilis* with an error rate of 24.37%, followed by the nonlinear hyperbolic model (25.38%). The R^2 values for all three models of *Q. variabilis* were greater than 0.90, whereas the R^2 for the fitted curve of *Q. acutissima* was 0.99 in the Ye model. In summary, the Ye model performed better than the rectangular hyperbola and the non-rectangular hyperbola models in terms of fitting the photosynthetic parameters (e.g., maximum net photosynthetic rate, light saturation point, and light compensation point). Further, its model evaluation index *RMSE* was lower, the R^2 was closer to one, and the fitting accuracy was higher. This signified that the Ye model was better suited for fitting the net photosynthetic light response curves of *Q. acutissima* and *Q. variabilis*.

4. Discussion

4.1. Relationships between Photosynthetic Rates and Eco-Physiological Factors

During the early and peak growing seasons, diurnal changes in the net photosynthetic rates of *Q. acutissima* and *Q. variabilis* were unimodal, which was consistent with Zhao et al. and Fan et al. [34,35], but they diverged from the study of Wang et al. [33]. These researchers thought that this was due to the stomatal conductivity, which limited the availability of CO_2 at higher temperatures [36]. During the peak growing season, the net photosynthetic rates of *Q. acutissima* and *Q. variabilis* were significantly greater than during the early growing season, which was consistent with the changes in leaf stomatal conductivity. The main factor that influenced the net photosynthetic rates of *Q. acutissima* and *Q. variabilis* was stomatal conductivity. Table 1 shows that the correlation coefficients between the stomatal conductivities and net photosynthetic rates of *Q. acutissima* and *Q. variabilis* were 0.89 and 0.75, respectively, during the early growing season, which increased to 0.98 and 0.94 during the peak growing season. This was consistent with the study of Liang, who found that the stomatal factor was the primary driver behind changes in the net photosynthetic rate [37]. Stomatal conductivity steadily increased with stomatal expansion from the early to peak growing seasons, which stimulated photosynthesis [38]. Atmospheric temperatures, vapor pressure deficits, and relative humidity can affect stomatal opening and closing [39] and indirectly affect the net photosynthetic rate. In addition to stomatal factors, stomatal opening and closing had an indirect impact on the photosynthetic rate. Photosynthetic active radiation in conjunction with stomatal factors were important external factors that influenced the net photosynthetic rates of *Q. acutissima* and *Q. variabilis*. Wu et al. discovered that photosynthetically active radiation had a greater impact on sunny plants such as *Q. acutissima* and *Pinus sylvestris* [40]. This was due to photosynthetically active radiation that induced the generation of adenosine triphosphate (ATP) and nicotinamide adenine dinucleotide phosphate (NADPH), which assimilated carbon in the dark reaction stage [41]. The photosynthetic rate and intercellular CO_2 concentrations were negatively associated, which indicated that more intense photosynthesis consumed additional CO_2 . This was because the intercellular CO_2 concentrations affected the photochemical efficiency of photosystem II [42]. The photosynthetic rate was significantly positively correlated with the transpiration rate, which was consistent with the study of Kim [43]. As stomata conductivity reflects the

extent to which stomata open, both photosynthesis and transpiration employ stomata as channels. Thus, both of them increased with higher stomata conductivity.

4.2. Comparison of Photosynthesis–Light Response Models

Currently, the rectangular hyperbola, nonrectangular hyperbola, and Ye models are the most commonly utilized photosynthesis light response models [44], and they play important roles in fitting photosynthetic light response curves, while also predicting photosynthetic parameters [9]. The Ye model can accurately reflect the inhibition of the net photosynthetic rate with higher light intensities during photosynthesis in *Q. acutissima* and *Q. variabilis*, while the rectangular hyperbola and nonrectangular hyperbola models cannot indicate the inhibition of photosynthesis under strong light conditions [45]. This is due to the mathematical expressions for the rectangular hyperbola and nonrectangular hyperbola models lacking the asymptote of the poles [46]. Thus, they cannot simulate the decreasing photosynthetic rate under higher light intensities. Conversely, the Ye model is based on the rectangular hyperbola model with the addition of correction parameters to bring the fitted curve closer to the actual measurement [30]. Deng et al. discovered that the Ye model fitted the *Q. variabilis* photosynthesis–light response curve better than the rectangular hyperbola or nonrectangular hyperbola models [22].

Since photosynthetic parameters reflect the capacity of plants to utilize light energy [45], the adaptabilities of the three models to the light response curves of *Q. acutissima* and *Q. variabilis* were compared. Both the rectangular hyperbola and nonrectangular hyperbola models had lower light saturation points than the actual curve, which was consistent with the studies of Xu and Xi [47,48]. This was due to the light saturation points of the rectangular hyperbola and nonrectangular hyperbola models not being directly obtainable, which had to be calculated using Richardson’s hypothetical empirical formula [49]. The light saturation point of *Q. acutissima* predicted by the Ye model was significantly lower than the measured value, while the predicted light saturation point of *Q. variabilis* was not significantly different from the measured value. This indicated that the prediction of the light saturation point of *Q. variabilis* using the Ye model was superior to that of *Q. acutissima*. The prediction of the light compensation point (LCP) for *Q. acutissima* and *Q. variabilis* via the three models revealed differences. The LCP of *Q. acutissima* predicted by the Ye model was closer to the measured curve than that of the rectangular hyperbola and nonrectangular hyperbola models, while the LCP of *Q. variabilis* predicted by the three models was not significantly different from that of the measured value. The differences between the models may have been due to the smaller LCP of *Q. acutissima*, which was more photonically sensitive under low light conditions [50]. The dark respiration rate of *Q. acutissima* predicted by the nonrectilinear hyperbolic model was closer to the measured value, while the dark respiration rates predicted by the rectangular hyperbola and Ye models were significantly larger than the measured values. This signified that the prediction of the dark respiration rate of *Q. acutissima* by the nonrectilinear hyperbolic model was better than those projected by the rectangular hyperbola and Ye models. The predicted dark respiration rates of *Q. variabilis* using the three models were not significantly different from the measured values, which indicated that all three models were suitable for fitting the *Q. variabilis* dark respiration rate.

4.3. Comparison of Net Photosynthetic Rates with Other Regions

In this study, the net photosynthetic rate of *Q. variabilis* was similar to that of the Funiu Mountain area but lower than that of this species on Taihang Mountain and other regions [49]. The net photosynthetic rate of *Q. acutissima* in this study was closer to that of Nanjing, Chuzhou, and Wanyuan [34,51] but lower than that of Fei County, Kunming [52]. According to Table 4, we found that higher precipitation translated to a lower net photosynthetic rate. Following 15 years of continuous observation of terrestrial ecosystems in Qinghai and Tibet, Xu et al. discovered that the net primary productivity decreased with higher precipitation [53]. Wang et al. found that the net photosynthetic rate of *Q. variabilis*

in northern habitats (Beijing) was significantly higher than in southern habitats (Yunnan), which received more precipitation [54]. Furthermore, acid rain had a significant impact on the net photosynthetic rate. Kunming, which has the same annual average temperature and precipitation, has a higher net photosynthetic rate than Nanjing and Jurong, which might have been due to the pH of the rainfall. Acid rain had a positive effect on the leaf photosynthetic rate when the pH was above 5.0 and had a negative effect when below this level [25]. It is known that the annual average precipitation pH value was 4.87 in the Changjiang River Delta [21] and 7.28 in Kunming city [55]. Thus, it was obvious that the pH of precipitation can inhibit photosynthesis in the oak forests of the Changjiang River delta. Differences in the photosynthetic capacities of *Q. variabilis* in different regions were also influenced by latitude. Xiong et al. discovered that latitude had a significant impact on *Q. variabilis* photosynthesis [56]. Liu et al. also found that, at high latitudes, *Q. variabilis* had higher dark respiration rates, whereas, at low latitudes, it had higher maximum net photosynthetic rates and lower light compensation points [57]. This was thought to be attributed to increases in the chlorophyll and nitrogen contents of *Q. variabilis* leaves with increasing latitude.

Table 4. Comparison of net photosynthetic rates of *Q. acutissima* and *Q. variabilis* in different regions. These data were obtained during July and August.

Species	Area	Daily MEAN Net Photosynthetic Rate/ $\mu\text{mol}\cdot\text{m}^{-2}\cdot\text{s}^{-1}$	Annual Rainfall/mm	Mean Annual Temperature/ $^{\circ}\text{C}$	Precipitation pH	Latitude/N	Climatic Zone	Reference
<i>Q. variabilis</i>	Funiu Mountain	3.26	1100	12~14.1	-	32°45'	Temperate	[49]
	Taihang Mountain	7.62	641.7	12.4~14.3	5.13	35°01'	Temperate	[35]
	Beijing	7.72	669.1	10.8	5.21	40°29'	Temperate	[54]
	Jurong	3.10	1055	15.2	4.87	32°07'	Subtropics	This study
<i>Q. acutissima</i>	Kunming	6.20	1035	15	7.80	-	Subtropics	[52]
	Feixian	6.79	856.4	20	5.35	117°96'	Temperate	[51]
	Chuzhou	3.65	1050	15	5.06	118°08'	Subtropics	[51]
	Wanyuan	3.67	1100	15	4.74	108°06'	Subtropics	[51]
	Nanjing	4.47	1100	15.1	4.87	31°35'	Subtropics	[34]
	Jurong	4.16	1055	15.2	4.87	31°59'	Subtropics	This study

4.4. Comparison of Photosynthetic Parameters between *Q. acutissima* and *Q. variabilis*

The daily average net photosynthetic rate of *Q. acutissima* was significantly greater than that of *Q. variabilis* during the early and peak growing seasons, and its maximum net photosynthetic rate (referring to photosynthetic potential) was also greater than that of *Q. variabilis*. This indicated that *Q. acutissima* possessed a stronger photosynthetic capacity and superior carbon sequestration efficiency. As the trees grew, the photosynthetic capacity of *Q. acutissima* differed even more significantly from that of *Q. variabilis*. The light compensation point reflects the photosynthetic capacity of plants under low light conditions. The light compensation point of *Q. acutissima* was significantly smaller than that of *Q. variabilis*, which implied that the photosynthetic capacity of *Q. acutissima* was superior under low light conditions. The dark respiration rate is an important parameter that characterizes plant respiration, where the higher the value, the more CO_2 is released. The dark respiration rate of *Q. acutissima* was $0.289 \text{ mol m}^{-2} \text{ s}^{-1}$, which was significantly lower than that of *Q. variabilis* ($1.553 \text{ mol m}^{-2} \text{ s}^{-1}$). This suggested that the number of carbohydrates consumed by *Q. acutissima* was smaller than that of *Q. variabilis*. Specifically, when all other conditions were equivalent, the quantity of CO_2 fixed by *Q. acutissima* was greater than that of *Q. variabilis*. In summary, *Q. acutissima* had a higher photosynthetic carbon sequestration capacity than *Q. variabilis*, which makes it a priority candidate species for carbon sink forests.

5. Conclusions

By synthesizing data from photosynthetic processes and fitting the photosynthetic light response curves, we assessed the photosynthetic characteristics of *Q. acutissima* and *Q. variabilis* and their photosynthetic efficiencies. Our results indicated the following: (1) The photosynthetic capacities of *Q. acutissima* and *Q. variabilis* significantly increase with their growth. (2) Stomatal conductivity was the most important physiological factor that affected photosynthesis in *Q. acutissima* and *Q. variabilis*, where photosynthetically active radiation was the most critical environmental factor. (3) The Ye model was the optimal model for fitting the light response curves of *Q. acutissima* and *Q. variabilis*. (4) The photosynthetic efficiency of *Q. acutissima* was higher than that of *Q. variabilis*; thus, it can serve as a priority species for carbon sink forests in the Changjiang River delta region. In the future, investigations into the processes and kinetics of acid rain that affect the photosynthesis of *Q. acutissima* and *Q. variabilis* need to be conducted, as does an evaluation of carbon fixation capacities in acid rain areas.

Author Contributions: Conceptualization, C.R. and H.H.; methodology, C.R.; software, C.R.; validation, C.R. and H.H.; formal analysis, C.R.; investigation, C.R., C.C., P.F., X.J., Z.W. and L.Z.; resources, C.R. and H.H.; data curation, C.R., C.C., P.F. and X.J.; writing—original draft preparation, C.R.; writing—review and editing, C.R. and H.H.; visualization, C.R.; supervision, H.H., Z.W. and L.Z.; project administration, C.R., H.H., Z.W. and L.Z.; funding acquisition, H.H. All authors have read and agreed to the published version of the manuscript.

Funding: This research was funded by a special fund project for Technology Innovation in Carbon Peak Carbon-Neutral in 2021 (BE2022305), the National Positioning Observation and Research Station of Forest Ecosystem in Yangtze River Delta (2020132077), and the Technical Collaboration Project on Soil Carbon and Nitrogen Migration Monitoring and Ecological Service Function of Soil and Water Conservation in Hilly Areas of Wuxi City (JSJGWXCG2022-09).

Institutional Review Board Statement: Not applicable.

Informed Consent Statement: Not applicable.

Data Availability Statement: The data that support the findings of this study are available in the supplementary material of this article.

Acknowledgments: We would like to thank Chan Wang and Xin Zhang for their assistance with field experiments and data collection. We also appreciate the technical support of the Xiashu Forest Farm.

Conflicts of Interest: The authors declare no conflict of interest. The funders had no role in the design of the study; in the collection, analyses, or interpretation of the data; in the writing of the manuscript; or in the decision to publish the results.

References

1. Tomimatsu, H.; Tang, Y. Effects of high CO₂ levels on dynamic photosynthesis: Carbon gain, mechanisms, and environmental interactions. *J. Plant Res.* **2016**, *129*, 365–377. [[CrossRef](#)]
2. Shi, X.; Wang, T.; Lu, S.; Chen, K.; He, D.; Xu, Z. Evaluation of China's forest carbon sink service value. *Environ. Sci. Pollut. Res. Int.* **2022**, *29*, 44668–44677. [[CrossRef](#)] [[PubMed](#)]
3. Zhou, H.; Yu, Q.; Kuang, Q.; Wang, W.; Wang, F.; Xu, H.-I. Light response of cut-flower Chrysanthemum cultivars. *J. Food Agric. Environ.* **2013**, *11*, 865–867.
4. Bhusal, N.; Bhusal, S.J.; Yoon, T.-M. Comparisons of physiological and anatomical characteristics between two cultivars in bi-leader apple trees (*Malus × domestica* Borkh.). *Sci. Hortic.* **2018**, *231*, 73–81. [[CrossRef](#)]
5. Shimada, R.; Takahashi, K. Diurnal and seasonal variations in photosynthetic rates of dwarf pine *Pinus pumila* at the treeline in central Japan. *Arct. Antarct. Alp. Res.* **2022**, *54*, 1–12. [[CrossRef](#)]
6. Jiang, Z.H.; Wang, C.S.; Zhang, J.; Yue, Y.; Li, S.W. Online monitoring and analysis of plant photosynthetic physiology and environmental factors. *Appl. Mech. Mater.* **2013**, *241*, 75–80. [[CrossRef](#)]
7. Schechter, P.L.; Wynne, R.A. Even Simpler Modeling of Quadruply Lensed Quasars (and Random Quartets) Using Witt's Hyperbola. *Astrophys. J.* **2019**, *876*, 9–12. [[CrossRef](#)]
8. Calama, R.; Puertolas, J.; Madrigal, G.; Pardos, M. Modeling the environmental response of leaf net photosynthesis in *Pinus pinea* L. natural regeneration. *Ecol. Model.* **2013**, *251*, 9–21. [[CrossRef](#)]

9. Fang, L.; Zhang, S.; Zhang, G.; Liu, X.; Xia, X.; Zhang, S.; Xing, W.; Fang, X. Application of Five Light-Response Models in the Photosynthesis of *Populus × Euramericana* cv. ‘Zhonglin46’ Leaves. *Appl. Biochem. Biotechnol.* **2015**, *176*, 86–100. [[CrossRef](#)]
10. Xia, J.B.; Zhang, G.C.; Wang, R.R.; Zhang, S.Y. Effect of soil water availability on photosynthesis in *Ziziphus jujuba* var. *spinosa* in a sand habitat formed from seashells: Comparison of four models. *Photosynthetica* **2014**, *52*, 253–261. [[CrossRef](#)]
11. Park, K.S.; Bekhzod, K.; Kwon, J.K.; Son, J.E. Development of a coupled photosynthetic model of sweet basil hydroponically grown in plant factories. *Hortic. Environ. Biotechnol.* **2016**, *57*, 20–26. [[CrossRef](#)]
12. Lang, Y.; Wang, M.; Zhang, G.C.; Zhao, Q.K. Experimental and simulated light responses of photosynthesis in leaves of three species under different soil water conditions. *Photosynthetica* **2013**, *51*, 370–378. [[CrossRef](#)]
13. Li, Y.L.; Liu, X.G.; Hao, K.; Yang, Q.L.; Yang, X.Q.; Zhang, W.H.; Cong, Y. Light-response curve of photosynthesis and model fitting in leaves of *Mangifera indica* under different soil water conditions. *Photosynthetica* **2019**, *57*, 796–803. [[CrossRef](#)]
14. Ye, Z.P.; Suggett, D.J.; Robakowski, P.; Kang, H.J. A mechanistic model for the photosynthesis-light response based on the photosynthetic electron transport of photosystem II in C3 and C4 species. *New Phytol.* **2013**, *199*, 110–120. [[CrossRef](#)] [[PubMed](#)]
15. Yuan, M.; Qu, L.; Wang, X.; Qian, Q.; Yang, W.; Wang, T.; Kong, H.; Jiang, G.; Chong, K. Research Advances on Plant Science in China in 2013. *Chin. Bull. Bot.* **2014**, *49*, 347.
16. Li, X.; Lu, Y.; Huang, A.; Yuan, R.; Li, J.; Hu, D.; Zhong, Q.; Cheng, D. Light response model fitting and photosynthetic characteristics of ten different fern species in subtropics. *Acta Ecol. Sin.* **2022**, *42*, 3333–3344.
17. Huang, Z.J.; Fan, Z.L.; Huang, Y.-T.; Quan, Q.M. Photoresponse Curve Model Research and Correlation Analysis of *Euphorbia marginata*. *Res. J. Biotechnol.* **2017**, *12*, 258–264.
18. Pan, H.; Feng, Y.; Li, Y. The comparison of light responses among four species of *Calligonum* L. in early autumn. In Proceedings of the 3rd International Conference on Agricultural and Biological Sciences (ABS 2017), Qingdao, China, 26–29 June 2017.
19. Han, M.K.; Kim, K.J.; Yang, K.C. Comparison of carbon storages, annual carbon uptake and soil respiration to planting types in urban park—The case study of Dujeong park in Cheonan city. *Korean J. Environ. Ecol.* **2014**, *28*, 142–148. [[CrossRef](#)]
20. Sun, S.; Che, T.; Li, H.; Wang, T.; Ma, C.; Liu, B.; Wu, Y.; Song, Z. Water and carbon dioxide exchange of an alpine meadow ecosystem in the northeastern Tibetan Plateau is energy-limited. *Agric. For. Meteorol.* **2019**, *275*, 283–295. [[CrossRef](#)]
21. Li, Q.y.; Liu, X.; Zhang, J.C. Changing trends of acid rain types in the Yangtze River Delta region. *J. Nanjing For. Univ. (Nat. Sci. Ed.)* **2021**, *45*, 168–174.
22. Deng, Y.P.; Lei, J.P.; Pan, L.; Wang, X.R. Model fitting of photosynthetic light-response curves in different *Quercus variabilis* provenances and its parameter comparison. *Chin. J. Ecol.* **2016**, *35*, 387–394.
23. Xu, F.; Guo, W.h.; Xu, W.h.; Wang, R.q. Effects of light intensity on growth and photosynthesis of seedlings of *Quercus acutissima* and *Robinia pseudoacacia*. *Acta Ecol. Sin.* **2010**, *30*, 3098–3107.
24. Xiong, S.; Wang, Y.; Chen, Y.; Gao, M.; Zhao, Y.; Wu, L. Effects of Drought Stress and Rehydration on Physiological and Biochemical Properties of Four Oak Species in China. *Plants* **2022**, *11*, 679. [[CrossRef](#)] [[PubMed](#)]
25. Dong, D.; Du, E.; Sun, Z.; Zeng, X.; de Vries, W. Non-linear direct effects of acid rain on leaf photosynthetic rate of terrestrial plants. *Environ. Pollut.* **2017**, *231*, 1442–1445. [[CrossRef](#)]
26. Guo, G.; Li, X.; Zhu, X.; Xu, Y.Y.; Dai, Q.; Zeng, G.R.; Lin, J. Effect of Forest Management Operations on Aggregate-Associated SOC Dynamics Using a Cs-137 Tracing Method. *Forests* **2021**, *12*, 859. [[CrossRef](#)]
27. Chen, X.; Sun, J.; Lyu, M.; Wang, M.; Hu, D.; Zhong, Q.; Cheng, D. Prediction of photosynthetic light-response curves using traits of the leaf economics spectrum for 75 woody species: Effects of leaf habit and sun-shade dichotomy. *Am. J. Bot.* **2021**, *108*, 423–431. [[CrossRef](#)]
28. Duan, L.M.; Yan, X.; Liu, T.X.; Wang, G.L.; Tong, X. Photosynthetic physiological characteristics of artificial populus in semi-arid area under multiple scenarios. *J. Soil Water Conserv.* **2019**, *33*, 213–220.
29. Lykins, S.; Scammon, K.; Lawrence, B.T.; Melgar, J.C. Photosynthetic light response of florican leaves of erect blackberry cultivars from fruit development into the postharvest Period. *Hortscience* **2021**, *56*, 347–351. [[CrossRef](#)]
30. Ye, Z.P.; Yu, Q. Comparison of new and several classical models of photosynthesis in response to irradiance. *J. Plant Ecology (Chin. Version)* **2008**, *32*, 1356–1361.
31. Wang, H.Z.; Han, L.; Xu, Y.L.; Niu, J.L.; Yu, J. Simulated photosynthetic responses of *Populus euphratica* during drought stress using light-response models. *Acta Ecol. Sin.* **2017**, *37*, 2315–2324.
32. Yu, Q.; Wang, Q.Y.; Liu, Z.G.; Zhang, M.R.; Zhang, S.Z.; Shen, Y.M. Comparison of the light response models of photosynthesis in leaves of *Magnolia sinostellata* under different light intensity and moisture conditions. *Chin. J. Ecol.* **2018**, *37*, 898–905.
33. Wang, X.; Tong, X.; Zhang, J.; Meng, P.; Xie, H.; Hu, H.; Li, J. Effects of photosynthesis on soil respiration of *Quercus variabilis* plantation in southern Taihang Mountain of northern China. *J. Beijing For. Univ.* **2021**, *43*, 66–76.
34. Zhao, W.R.; Liu, X.; Zhang, J.C.; Wang, Y.X.; Wang, J.P.; Zhuang, J.Y. Photosynthesis transpiration, the carbon fixation and oxygen release, and the cooling and humidificand capacity of typical tree species in Nanjing suburban. *Sci. Silvae Sin.* **2016**, *52*, 31–38.
35. Fan, Y.; Hu, N.; Ding, S.; Lu, X. Physiological and ecological characteristics of photosynthesis of *Quercus variabilis* of different development stages in the funi mountain national nature reserve. *J. Ecol. Rural Environ.* **2015**, *31*, 684–689.
36. Zhang, Y.J.; Meinzer, F.C.; Qi, J.H.; Goldstein, G.; Cao, K.F. Midday stomatal conductance is more related to stem rather than leaf water status in subtropical deciduous and evergreen broadleaf trees. *Plant Cell Environ.* **2013**, *36*, 149–158. [[CrossRef](#)] [[PubMed](#)]
37. Liang, G.; Bu, J.; Zhang, S.; Jing, G.; Zhang, G.; Liu, X. Effects of drought stress on the photosynthetic physiological parameters of *Populus euramericana* “Neva”. *J. For. Res.* **2019**, *30*, 409–416. [[CrossRef](#)]

38. Wu, B.J.; Liu, Y.J.; Jiang, C.D.; Shi, L. Effects of stomatal development on leaf temperature during leaf expansion. *Plant Physiol. J.* **2015**, *51*, 119–126.
39. Ruan, C.X.; Hu, H.B.; Ji, J.; Ma, B.; Liu, X.L. Transpiration regulations and responses to climate factors of *Quercus acutissima* and *Quercus variabilis* in the Changjiang River delta area. *J. Soil Water Conserv.* **2021**, *35*, 338–344.
40. Wu, T.G.; Zeng, G.Q.; Xiao, Y.G.; Yao, J.; Yu, M.K.; Cheng, X.R.; Wang, C. Daily variation of photosynthesis of six tree species under *Pinus elliotii* forest and their relations with environmental factors. *J. Nanjing For. Univ. (Nat. Sci. Ed.)* **2011**, *35*, 135–138.
41. Feng, L.G.; Feng, Z.; Zhao, L.Y.; Sheng, L.X. Comparison of photosynthetic characteristics between wild plants and cultivars of *Rosa rugosa*. *Sci. Silvae Sin.* **2007**, *43*, 31–36.
42. Bhusal, N.; Kim, H.S.; Han, S.-G.; Yoon, T.-M. Photosynthetic traits and plant—Water relations of two apple cultivars grown as bi-leader trees under long-term waterlogging conditions. *Environ. Exp. Bot.* **2020**, *176*, 141–153. [[CrossRef](#)]
43. Kim, D.-H.; Jung, J.-Y.; Lee, C.-H.; Park, B.-D.; Bae, K.-H.; Kim, K.W.; Kim, P.-G. Effect of transpiration on the physiological vitality of *Zelkova serrata*. *For. Sci. Technol.* **2020**, *16*, 154–160. [[CrossRef](#)]
44. Leng, H.B.; Qin, J.; Ye, K.; Feng, S.C.; Gao, K. Comparison of light response models of photosynthesis in *Nelumbo nucifera* leaves under different light conditions. *J. Appl. Ecol.* **2014**, *25*, 2855–2860.
45. Chen, Z.Y.; Luo, F.Y.; Peng, Z.S.; Yu, M.Q. Comparison between modified exponential model and common models of light-response curve. *J. Plant Ecol. (Chin. Version)* **2012**, *36*, 1277–1285. [[CrossRef](#)]
46. Ye, Z.P. A review on modeling of responses of photosynthesis to light and CO₂. *J. Plant Ecol. (Chin. Version)* **2010**, *34*, 727–740.
47. Xu, G.C.; Luo, W.B.; Li, H.W.; Xu, Y.Q.; Ji, R.C.; Li, G.L.; Lin, Z.M.; Qiu, S.X.; Tang, H. Light response model and photosynthetic parameters of colored potatoes. *Fujian J. Agric. Sci.* **2020**, *35*, 691–698.
48. Xie, F.; Yan, Q.Q.; Yang, F.; Hou, Y.L. Photosynthetic Light Response Curve and Its Model Fitting of *Sophora davidii* from Different Provenances. *J. Temp. For. Res.* **2020**, *3*, 44–49.
49. Richardson, A.D.; Berlyn, G.P. Changes in foliar spectral reflectance and chlorophyll fluorescence of four temperate species following branch cutting. *Tree Physiol.* **2002**, *22*, 499–506. [[CrossRef](#)]
50. Sui, X.-l.; Mao, S.-l.; Wang, L.-h.; Zhang, B.-x.; Zhang, Z.-x. Effect of Low Light on the Characteristics of Photosynthesis and Chlorophyll a Fluorescence During Leaf Development of Sweet Pepper. *J. Integr. Agric.* **2012**, *11*, 1633–1643. [[CrossRef](#)]
51. Wang, B.; Yu, M.-K.; Sun, H.-J.; Cheng, X.-R.; Shan, Q.-H.; Fang, Y.-M. Photosynthetic characters of *Quercus acutissima* from different provenances under effects of salt stress. *Chin. J. Appl. Ecol.* **2009**, *20*, 1817–1824.
52. Chen, D.; Ou, G.; Chen, J.; Liu, G.; Li, Q.; Zhang, S.; Zhen, Y. Effects of different weather conditions on photosynthetic characteristics of juvenile plantations of four afforestation tree species in Yunnan Province. *J. Southwest For. Univ.* **2016**, *36*, 32–38.
53. Xu, J.; Chen, H.; Shang, S.; Yang, H.; Zhu, G.; Liu, X. Response of net primary productivity of Tibetan Plateau vegetation to climate change based on CEVSA model. *Arid Land Geogr.* **2020**, *43*, 592–601.
54. Wang, X.; Gao, W.; Liu, J.; Ni, Y.; Qu, L.; Zhao, X.; Yang, W.; Deng, Y.; Jiang, Z. Effects of habitat change on the photosynthetic characteristics of *Quercus variabilis* seedlings. *Acta Ecol. Sin.* **2016**, *36*, 8062–8070.
55. Huang, L.J.; Wang, D.X.; Wang, J.P. Characteristics and variations analysis on chemical composition of atmospheric precipitation of Kunming. *Environ. Sci. Surv.* **2022**, *41*, 46–48.
56. Xiong, D. Study on the Environmental Response to Ecophysiological Features of *Quercus variabilis* Seedlings. Master's Thesis, Huazhong Agricultural University, Wuhan, China, 2011.
57. Liu, J.F.; Xiao, W.F.; Xiong, D.P.; Lei, J.P.; Wang, P.C. Comparison on the physio-ecological characteristics of *Quercus variabilis* seedlings from various latitude sites. *Bull. Bot. Res.* **2011**, *31*, 467–471.